Near-Unity Efficiency Energy Transfer from Colloidal Semiconductor Quantum Wells of CdSe/CdS Nanoplatelets to A Monolayer of MoS_2

Nima Taghipour, [†] *Pedro Ludwig Hernandez Martinez,* [†, ‡] *Ayberk Ozden,* [§] *Murat Olutas,* [†, ¥] *Didem Dede,* [†] *Kivanc Gungor,* [†] *Onur Erdem,* [†] *Nihan Kosku Perkgoz* [Δ] *and Hilmi Volkan Demir* [†, ‡, #]

[†]Department of Electrical and Electronics Engineering, Department of Physics, UNAM-Institute of Materials Science and Nanotechnology, Bilkent University, Ankara 06800, Turkey

[‡] Luminous! Center of Excellence for Semiconductor Lighting and Displays, School of Electrical and Electronic Engineering, School of Physical and Materials Sciences, School of Materials Science and Nanotechnology, Nanyang Technological University, Singapore 639798, Singapore

[§] Department of Materials Science and Engineering, Faculty of Engineering, Anadolu University, 26555 Eskisehir, Turkey

[¥] Department of Physics, Abant Izzet Baysal University, Bolu 14030, Turkey

[Δ] Department of Electrical and Electronics Engineering, Faculty of Engineering, Anadolu University, 26555 Eskisehir, Turkey

[#]Corresponding author: volkan@stanfordalumni.org

Abstract

A hybrid structure of the quasi-2D colloidal semiconductor quantum wells assembled with a single-layer of 2D transition metal dichalcogenides offers the possibility of highly strong dipole-to-dipole coupling, which may enable extraordinary levels of efficiency in Förster resonance energy transfer (FRET). Here, we show ultra-high efficiency FRET from the ensemble thin films of CdSe/CdS nanoplatelets (NPLs) to a MoS_2 monolayer. From time-resolved fluorescence spectroscopy, we observed the suppression of the photoluminescence of the NPLs corresponding to the total rate of energy transfer from ~ 0.4 to 268 ns^{-1}. Using an Al_2O_3 separating layer between CdSe/CdS and MoS_2 with thickness tuned from 5 to 1 nm, we found that FRET takes place 7 to 88-fold faster than the Auger recombination in CdSe-based NPLs. Our measurements reveal that the FRET rate scales down with d^{-2} for the donor of CdSe/CdS NPLs and the acceptor of MoS_2 monolayer, d being the center-to-center distance between this FRET pair. A full electromagnetic model explains the behavior of this d^{-2} system. This scaling arises from the delocalization of the dipole fields in the ensemble thin film of the NPLs and full distribution of the electric field across the layer of MoS_2. This d^{-2} dependency results in an extraordinary long Förster radius of ~ 33 nm.

KEYWORDS: *nonradiative energy transfer, FRET, colloidal nanoplatelets, molybdenum disulphide, distance dependency, Förster radius, Auger recombination*

Two-dimensional (2D) materials, also known as van der Waals materials, show diverse electronic structures and properties. Among them are examples of transition metal dichalcogenide (TMDC) semiconductors (*e.g.*, molybdenum disulphide, MoS_2),[1] semimetals (*e.g.*, graphene)[2] and insulators (*e.g.*, hexagonal boron nitride, hBN).[1] Specifically, semiconducting TMDC 2D crystals including MoS_2 and WSe_2 exhibit very strong light-matter interaction.[3] For instance, MoS_2 monolayer can absorb as much as 10% of the normal incidence light at its excitonic peaks (615 and 660 nm).[1,2] This strong optical interaction has attracted great attention for applications in optoelectronics,[3–5] nanophotonics[2,5] and sensing.[6–8] More recently, another important class of semiconductors with their quasi-2D structure, colloidal quantum wells (CQWs), the so-called nanoplateletes (NPLs), which are most commonly synthesized in the form of CdX (where X represents S, Se and Te), have attracted interest for the ability to precisely control their vertical thickness.[9–11] Owing to the strong quantum confinement in the vertical direction, these semiconductor NPLs demonstrate attractive optical properties including giant oscillator strength, and narrow photoluminescence (PL) emission (purely homogenous broadening).[11–14] These interesting properties of the NPLs make them a highly promising material platform for efficient light-emitting diodes (LEDs),[15] lasers,[11,12] and photovoltaic devices.[16,17]

Nonradiative energy transfer (NRET) is an electromagnetic process of the energy transfer from a donor to an acceptor by near-field dipole-dipole coupling. One type of NRET is Förster resonance energy transfer (FRET),[18,19] where the rate of the excitation energy transfer essentially depends on the distance between the donor and the acceptor as well as the spectral overlap between the PL spectrum of the donor and the optical absorption spectrum of the acceptor, the absorption cross-section of the acceptor, PL quantum yield (QY) of the donor, and orientation of the dipoles between the donor and the acceptor.[18–20] FRET process has been shown to be effectively enhance the

performance of the light-generation, -harvesting and -sensing functions in specially designed hybrid structures. To date, numerous FRET studies have been conducted using colloidal semiconductor nanocrystals with different degrees of quantum confinement (quantum dots (QDs), nanorods (NRs), NPLs).[20] For example, FRET has been investigated in a hybrid structure of two types of NPLs, each with a different vertical thickness.[21,22] Thanks to their large absorption cross-section, NPLs emerged as a highly promising candidate for absorbing photons and photogenerating excitons potentially to be transferred *via* FRET. To this end, graphene,[23,24] graphene oxide[25,26] and carbon nanotubes[27] have been used as a sinking medium of the excitons. Especially, TMDC semiconductors including MoS_2[28,29] and $MoSe_2$[30] have exhibited high capability of exciton sinking from neighboring nanoemitters. For example, the FRET pairs of CdSe/CdS QD-donors with $MoSe_2$-acceptors[30] and of CdSe/CdS QD-donors with graphene-acceptors,[31] which are shown to exhibit the distance scaling of d^{-4}, have previously been reported. However, to the best of our knowledge, FRET has not been explored in the hybrid structure of the 2D NPLs and TMDC, although such a combination is very favorable because of their intrinsic geometrical similarity. Owing to their atomically flat topologies, the layer-to-layer dipole-dipole interaction between NPLs and TMDC films would be expected to achieve ultraefficient FRET compared to any other possible combinations of nanocrystal semiconductors and 2D materials.

In the present study, we report FRET from solid assembled thin films of colloidal CdSe/CdS core/crown NPLs serving as the donor to a single layer of MoS_2 serving as the acceptor. Here, we systematically study the FRET process and surprisingly find the rate of the FRET decays as $1/d^2$, where d is the distance between the donor NPL and acceptor TMDC 2D-structures. Although the decay rate is expected to scale with $1/d^4$, we reveal that the strong filed screening and the dipole electric field delocalization at the donor play major role for modifying the decay kinetics. To study

systematically FRET as function of the distance between the NPL nanoemitters and MoS_2 monolayer, we deposited thin films of dielectric spacers of alumina (Al_2O_3) with tuned thicknesses between the donor and the acceptor precisely controlled using atomic layer deposition (ALD) and employed the time-resolved fluorescence (TRF) spectroscopy to investigate the resulting luminescence decays of the NPLs. According to the measurements, the PL curves of the NPLs were significantly accelerated with decreasing thickness of Al_2O_3, which convincingly indicates the existence of the energy transfer. Subsequently, we found that by decreasing the spacer thickness to 1 nm, we achieved near-unity energy transfer efficiency of 99.88% with the ultrafast FRET lifetime of 3.73 ps at room temperature. Additionally, we support our findings with a full numerical electromagnetic model of the hybrid structure by simulating the dipole interaction within the model structure. We believe that this proposed system can offer interesting opportunities to achieve highly efficient photovoltaics devices, ultralow-threashod colloidal lasers and photocatalytics.

Results and Discussion

The synthesized 4 monolayer (ML) CdSe/CdS core/crown nanoplatelets (see Supporting Information for details) were transferred onto the pre-cleaned substrates *via* spin-coating. To study the distance dependency of energy transfer between the donor and the acceptor, thin films of Al_2O_3 were deposited on the top of a monolayer of MoS_2 *via* ALD technique. We measured the thickness of Al_2O_3 layer using ellipsometry technique (see Supporting Information, Figure S3). The thickness of the MoS_2 films was attained *via* atomic force microscopy (AFM) and we further performed Raman spectroscopy to verify the monolayer formation of MoS_2 flakes. (see Supporting Information, Figure S2). Figure 1a shows the schematic representation of the fabricated hybrid

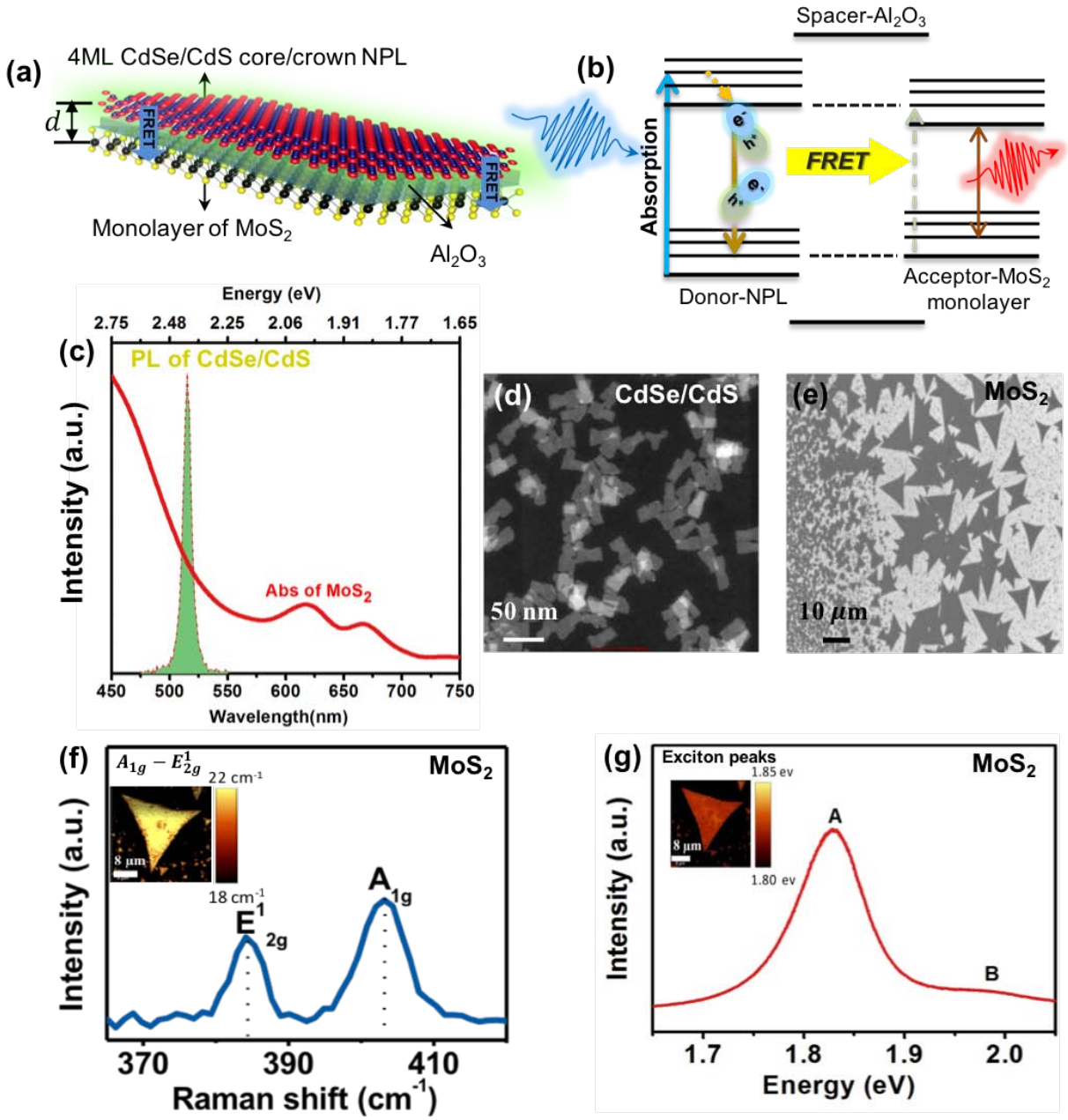

Figure 1. (a) Graphical illustration of the hybrid assembled films of NPLs-Al_2O_3-MoS_2 (donor- spacer-acceptor) system. (b) Schematic representation of the FRET process where the energy band diagram indicates the transfer of excitons. **(**c) Normalized photoluminescence of the 4ML CdSe/CdS core/crown NPLs (donor) and UV-vis absorption spectrum of the MoS_2 triangular monolayer flakes (acceptor). (d) High-angle annular dark field transmission microscopy image of the NPLs. (e) Scanning electron microscopy image of the MoS_2 film. (f) Raman spectrum of the MoS_2 film. The inset shows the $A_{1g} - E^1_{2g}$ central map of Raman spectra. (g) PL spectrum of the MoS_2 film. The inset exhibits the spatial map of exciton peak around 1.83 eV.

structure of the 4 monolayer CdSe/CdS core/crown NPLs and MoS_2 monolayer, which are separated from each other with the dielectric thin films of Al_2O_3 having thickness tuned from 1 to 40 nm. Here in, d is the center-to-center distance between the donor and the acceptor dipoles (where $d = d_L + t_{NPL}/2 + t_{Al_2O_3}$ where the d_L is the length of oleic acid (calculated in the range of 1.95-1.99 nm),[32,33] t_{NPL} is the thickness of NPLs (taken as 1.2 nm for 4 ML CdSe core NPLs)[32,33] and $t_{Al_2O_3}$ is the thickness of Al_2O_3). Figure 1b schematically illustrates the FRET process between the donor and the acceptor where the excited donor (D^*) relaxes to its ground state (D) while the excitation energy is transferred to the acceptor, which it is in the ground state (A) before the energy transfer is occurred. ($D^* + A \xrightarrow{\boldsymbol{FRET}} D + A^*$). In our particular study, D is the CdSe/CdS NPL with 4 monolayers, while A is the single MoS_2 monolayer. Figure 1c shows the spectral overlap between the PL spectrum of the donor and the UV-vis absorption spectrum of the acceptor. PL spectrum of the NPLs peaks at 518 nm with a full-width at half maximum (FWHM) of 8 nm and the two peaks in the absorption spectrum of MoS_2 around 1.83 and 2.0 eV, corresponding to *A* and *B* excitonic peaks, respectively. From the high-angle annular dark field transmission electron microscopy (HAADF-TEM) images of the NPLs (Figure 1d), the average length and width are calculated to be 34.37 ± 2.21 nm and 15.67 ± 1.29 nm, respectively. Figure 1e depicts the scanning electron microscopy (SEM) image of the isolated MoS_2 triangular flakes where the surface coverage of these islands reaches up to 80%. The Raman shifts and the PL spectrum of the MoS_2 flakes are presented in Figure 1f and 1g, respectively. The inset of Figure 1f exhibits the $A_{1g} - E^1_{2g}$ Raman mode difference map, which is in the range of 18 to 22 cm^{-1}, typical for MoS_2 flakes.[34,35] Furthermore, the PL spectrum (Figure 1g) and *A* exciton peak center map (the inset of Figure 1g) exhibit the *A* and *B* exciton peaks and a bandgap of ~1.83 eV, respectively, confirming the growth of MoS_2 monolayer.[36] In addition, we further determined the

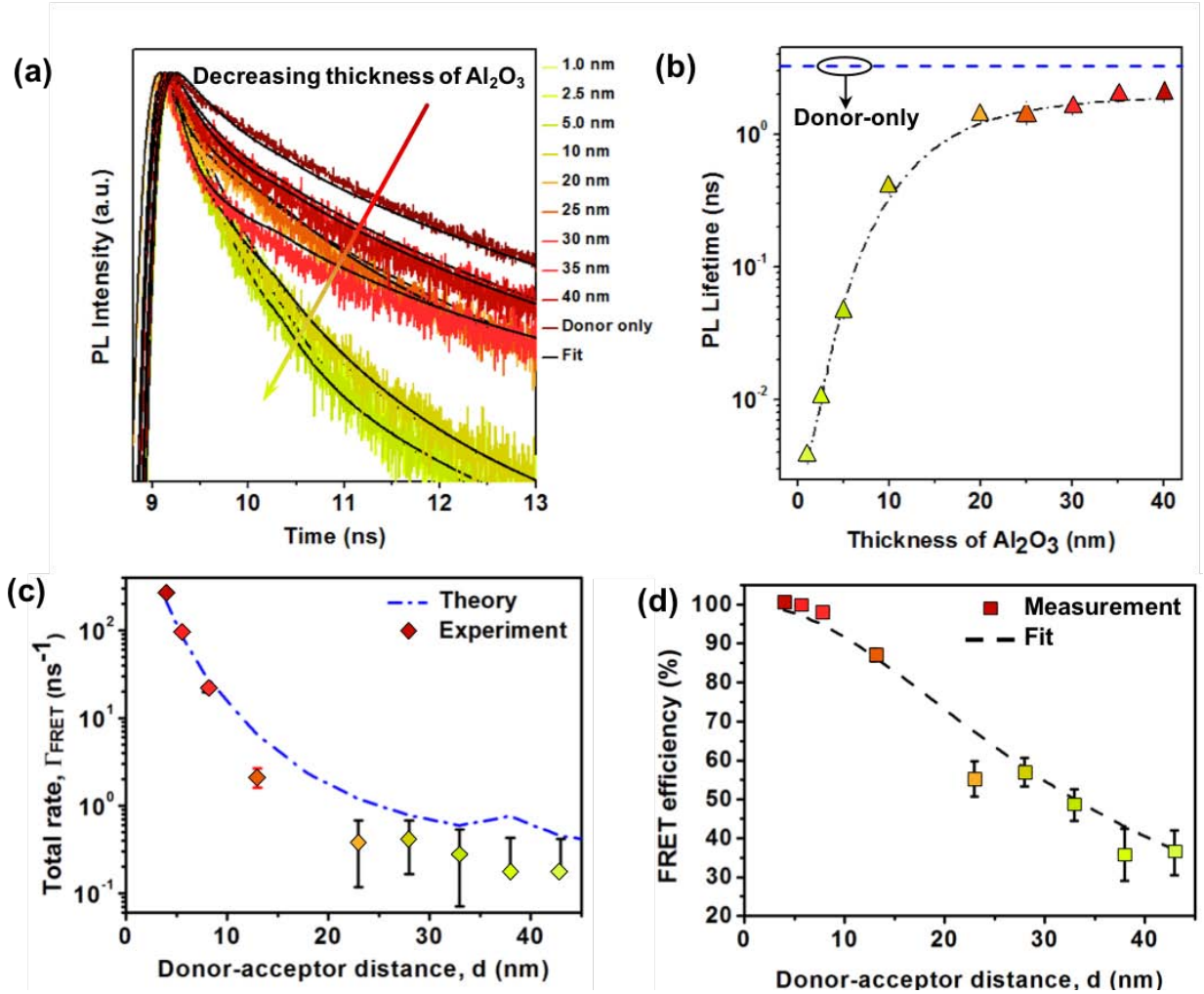

Figure 2. (a) Photoluminescence decay curves of the solid films of the NPLs-MoS_2 assembly, collected at the donor PL emission peak with varying thicknesses of the Al_2O_3 separation layer. The solid black lines represent the fits of the curves. (b) Evolution of amplitude-averaged lifetime of the solid film samples at PL emission peak wavelength of the donor as a function of the spacer layer thickness. The blue dashed-line indicates the only donor PL lifetime. (c) Total rate of FRET as function of the Al_2O_3 thin-film thickness (separation thickness). The blue dot-dashed line is electromagnetic behavior of the system (COMSOL electromagnetic numerical simulation). (d) Efficiency of FRET as a function of the center-to-center distance between the donor and the acceptor. The dashed line is the numerical fitting.

thickness of MoS_2 flakes *via* atomic force microscopy (Supporting Information, Figure S2), which corroborates the formation of the single layer flakes.

TRF decays of the donor PL bandedge emission (at 518 nm) are shown in Figure 2c for varying separating thickness of the dielectric layer. To verify that the NPLs are distributed homogeneously on the films, we performed the TRF measurements at the different positions on the samples and observed that the PL decay curves are very similar in each position (see Supporting Information,

Figure S4 and Tables S1-S10). Here, the donor-only sample, in which the NPLs were deposited alone on a pre-cleaned Al_2O_3-SiO_2-Si substrate where the thickness of Al_2O_3 is 5 nm, acts as the reference sample.

As can be seen in Figure 2a, by decreasing the distance between the donor and the acceptor, PL decay kinetics of the NPLs significantly changes and becomes progressively faster, which indicates that a new channel is opened up for relaxation of the carries. This transition can be attributed to FRET or charge transfer between the donor and the acceptor. However, in our solid system, the surfaces of the NPLs are passivated by well-known nonaromatic ligand (oleic acid). Additionally, the donor and the acceptor are separated with full-coverage from each other by the ALD-grown spacer. Therefore, the charge transfer is ineffective in our hybrid structure, which is also fully consistent with previous experimental studies.[27,29,37]

To analyze PL decay kinetics of the donor in the presence of the acceptor, PL decay curves were fitted by multi-exponential functions, and their lifetime components and amplitude-weighted contributions are summarized in Tables S1-S10. (See Supporting Information.) The amplitude-average lifetime (τ_{av}) is plotted as a function of the Al_2O_3 thickness in Figure 2d.

If the lifetime of the donor in the absence of acceptor is τ_D and the lifetime of the donor in the presence of the acceptor is τ_{DA}, the total FRET rate (Γ_{FRET}) can be considered as $\Gamma_{FRET} = 1/\tau_{FRET} = 1/\tau_{DA} - 1/\tau_D$.[28,38–40] Figure 2c shows Γ_{FRET} calculated from the experimental measurements. Furthermore, we numerically computed Γ_{FRET} using an electromagnetic model where the donor is represented as radiating dipoles in *x*, *y*, and *z* orientation inside each NPL in the presence of lossy media modeled as a layer of MoS_2 placed between Al_2O_3 (used as the separating film) and SiO_2 (taken as the substrate). The total theoretical FRET rate was obtained by the arithmetic mean of FRET rates in the three orientations, given as the dash-dotted blue line in Figure

2c. The experimental Γ_{FRET} was found to be 268.06 ns^{-1} for the sample having 1 nm thickness. To the best of our knowledge, this attained Γ_{FRET} is the highest value that has been reported thus far in this kind of structure when compared to the previous studies.[24,26–29] Consequently, as presented in Figure 2c, using a Al_2O_3 separating layer with thickness below 5 nm, FRET occurs in an ultrafast timescale corresponding to 3.73- 46.40 ps (see Figure 2b). These ultrafast FRET times overcome the Auger recombination process in NPLs, which is in the range of hundreds of picoseconds (150-500 ps) for CdSe NPLs,[21] making these hybrid FRET structure potentially interesting for the purpose of reducing optical gain threshold in lasing systems and increasing charge extraction performance in multiexcitonic photovoltaics.

Figure 2c depicts the numerical calculated FRET rate using COMSOL along with the experimental FRET rate extracted from TRF donor PL lifetimes. We see good agreement between the experimental observation and our classical electromagnetic model (see below for more details about the numerical calculations). In this figure, we observe that for distances larger than 20 nm, both the experimental and numerical FRET rates have an oscillating behavior. We attribute this oscillation to the electric field interference coming when the dipoles are placed on the top of dielectric surface. Figure 2d illustrates the FRET efficiency (η_{FRET}) of the samples, which are calculated by $\eta_{FRET} = 1 - (\tau_{DA}/\tau_D)$ as a function of the donor-acceptor distance (d). Here we find near-unity (99.88%) FRET efficiency for d = 3.57 and 5.07 nm. In addition, we further investigated the FRET rate distance dependency using the expression $\eta_{FRET} = 1/(1 + \left(\frac{d}{d_0}\right)^n)$, where d_0 is the Förster radius and n is the parameter that indicates the FRET distance dependency. By fitting the experimental data numerically, we extract a Förster radius of d_0 =32.97 ± 0.15 nm and n = 2 order value (the numerical fitting for n = 4 which is the extracted order dependence for two dimensional acceptors, is given in Figure S5). n = 2 indicated that distance dependency of the

interaction results from layer-to-layer dipole-dipole coupling.[18,27,38–44] Consequently, the FRET distance dependency of $1/d^2$ leads to further extend the FRET radius to longer distances (> 10 nm) as compared to $1/d^4$ (the case of two dimensional structures) and $1/d^6$ (the case of zero dimension structures, *i.e.*, point to point).[38,40] It is worth mentioning that the Förster radius ~ 32.97 nm is the longest that has been reported in literature thus far, to the best of our knowledge.

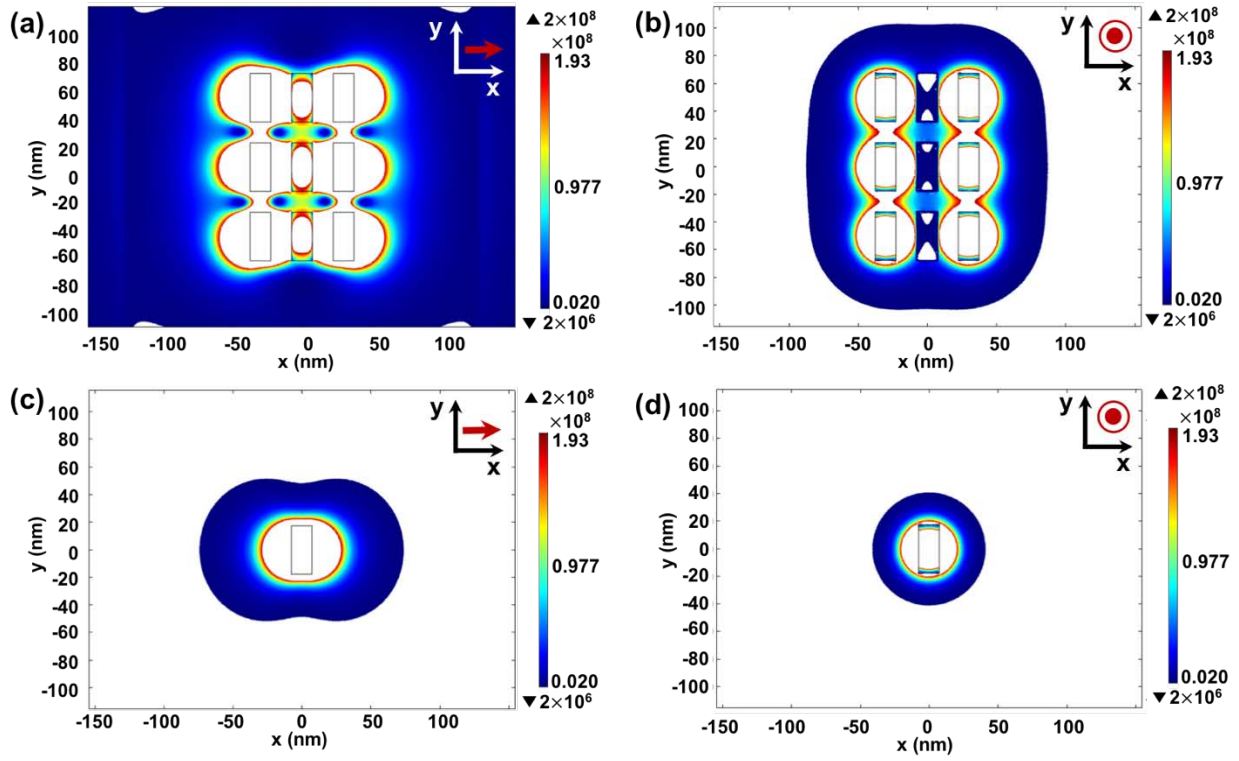

Figure 3. Electric field intensity ($\mathbf{E}^2$) distribution at the NPL site: a) for several NPLs when the dipoles are oriented in the *x* axis and b) in the *z* axis, and c) for single NPL when the dipole is oriented in the *x* axis, and d) in the *z* axis.

To support the experimental results, we numerically computed the FRET rate. First, we assumed that an exciton dipole is placed inside several NPLs, and MoS_2 monolayer acts as exciton absorber medium (Figure 1a). Then, the FRET rate, Γ_{FRET}, for an exciton dipole with orientation α, is calculated by:[45,46]

$$\Gamma_{FRET} = \frac{2}{\hbar}\frac{\mathrm{Im}\left(\varepsilon_{MoS2}\left(\omega_{exc}\right)\right)}{4\pi}\int_{MoS_2}\mathbf{E}\bullet\mathbf{E}^{*}dV \qquad (1)$$

where $\varepsilon_{MoS_2}(\omega_{exc})$ is the MoS_2 dielectric function at the exciton frequency of the NPL and $\mathbf{E}$ is the electric field induced by an oscillating exciton dipole $\mu e^{-i\omega_{exc}t}$. The integral was taken over the MoS_2 layer.

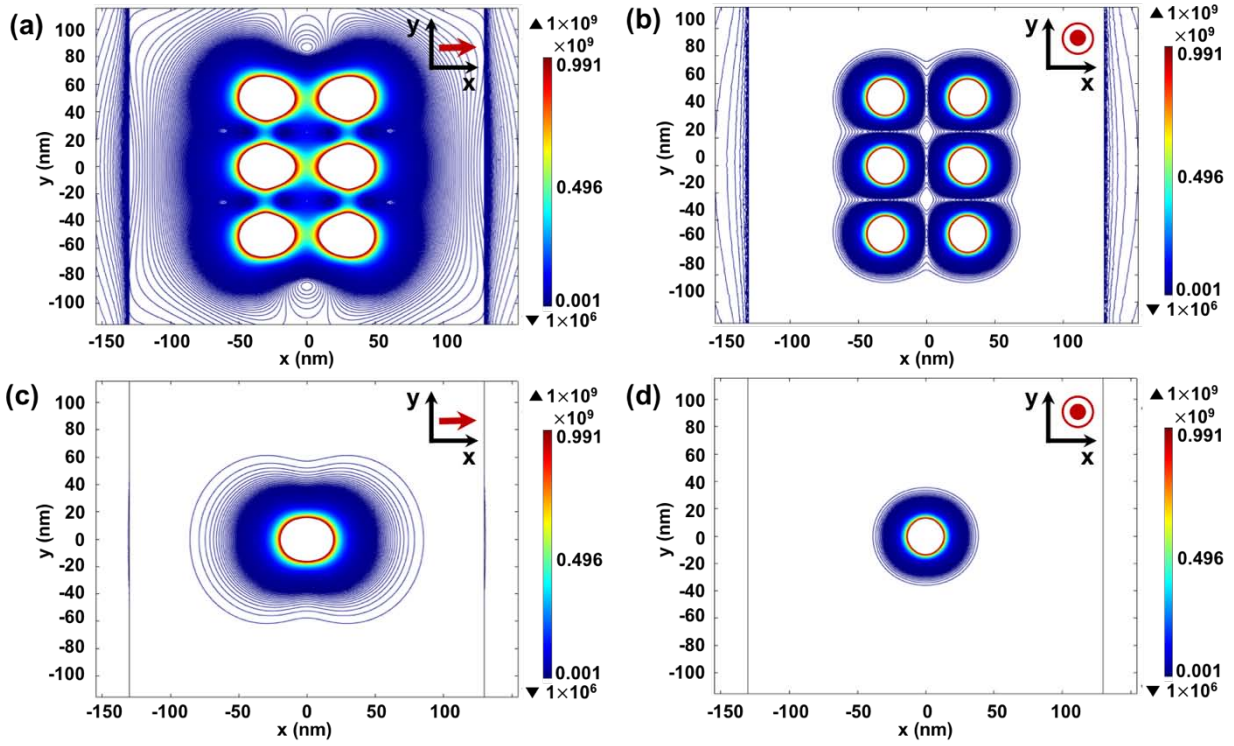

Figure 4. Electric field intensity ($\mathbf{E}^2$) distribution at MoS_2 layer for 1 nm separation layer: a) for several NPLs when the dipoles are oriented in the *x* axis and b) in the *z* axis, and c) for single NPL when the dipole is oriented in the *x* axis and d) in the *z* axis.

The electric field was calculated using COMSOL, where the oscillating dipoles were placed inside the NPLs, and then the field induced subsequently in the MoS_2 layer was computed. The transfer rate, Γ_{FRET}, was calculated by using Eq 1 for different orientations of the dipole. Figure 3 shows the electric field intensity at the NPL site. As can be observed, E^2 is distributed along the layer of NPLs, which results from the delocalization of the dipoles. However, in the case of a single NPL, the field is mainly localized around the NPL.

Figure 4 shows the electric field intensity in the MoS_2 layer together with a 1 nm thick separation layer between the donor and the acceptor. It can be seen that the electric field for a *x* dipole is more delocalized as compared to a dipole oriented in the *z* axis. We attribute this behavior to the screening effect resulting from the dipole orientation. Figure 5 shows the electric filed intensity distribution at MoS_2 layer when the dipole is oriented in the *x* and *z* axes using a 30 nm thick spacer. As can be observed from this figure, the electric field intensity is more distributed across

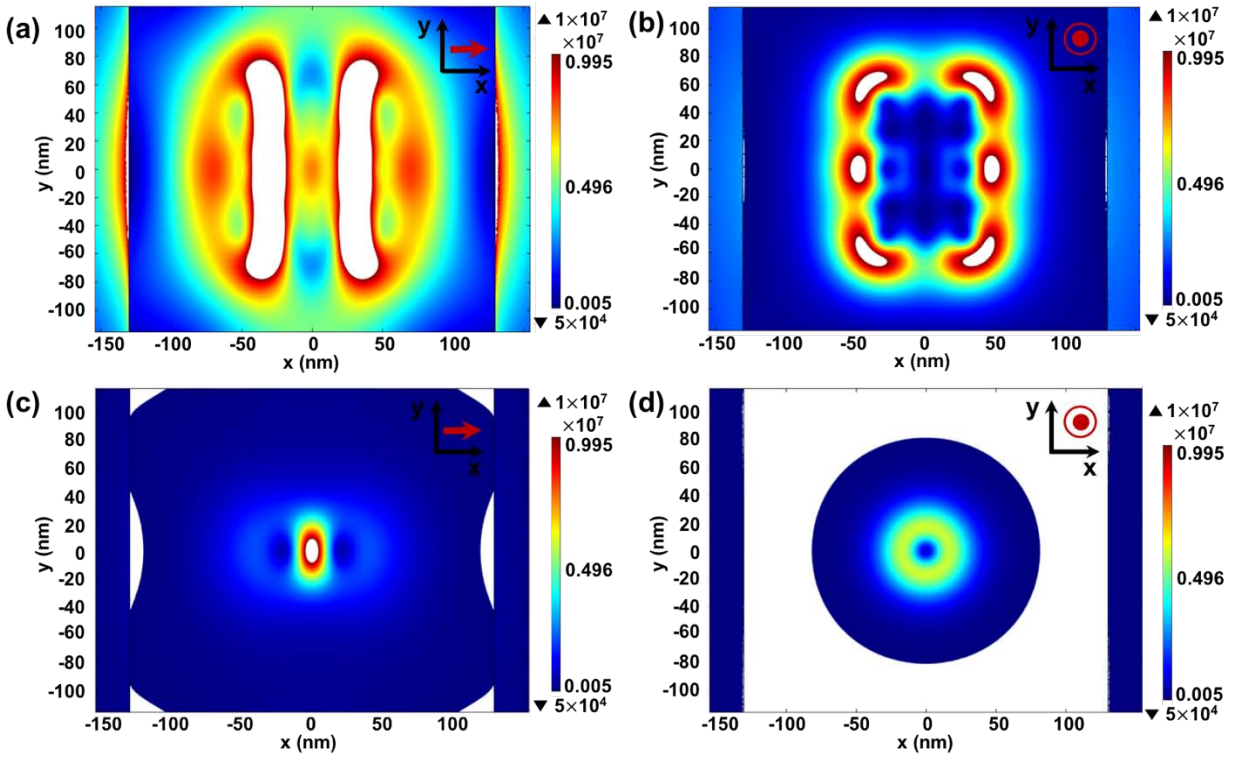

Figure 5. Electric field intensity ($\mathbf{E}^2$) distribution at MoS_2 layer for a 30 nm thick separation layer: a) for several NPLs when the dipoles are oriented in the *x* axis and b) in the *z* axis, and c) for single NPL when the dipole is oriented in the *x* axis and d) in the *z* axis.

the MoS_2 in the case of several NPLs as compared to the single NPL where the electric field is more localized. Moreover, the electric field intensity is an order of magnitude larger for the *x*-oriented dipole than the *z*-oriented dipole, which emphasizes the anisotropic behavior of the CdSe based NPLs dipoles, as shown in the previous studies.[47,48] Thus, we can imply that the main

contribution for the FRET rates comes from the *x*- and *y*-oriented dipoles. Therefore, the exciton delocalization along the NPLs and the electric field intensity distributed along the MoS_2 acceptor layer support the FRET rate leading to the $1/d^2$ decay.[18,27,38–44]

Conclusions

In conclusion, we have experimentally showed a Förster-type nonradiative energy transfer in the hybrid structure of CdSe/CdS NPLs and MoS_2 monolayer thin film assembled together. We found near-unity FRET efficiency reaching 99.88% with an ultrafast FRET rate of 268.06 ns^{-1}. Owing to the layer-to-layer dipole coupling between the CdSe/CdS donor and the MoS_2 acceptor, the rate of FRET follows the d^{-2} scaling. This dependency is supported with a full numerical electromagnetic model, which shows that the d^{-2} behavior comes from the delocalization of the electric field distribution across the layers of NPLs and MoS_2. In addition, the d^{-2} dependency further extends the Förster radius to a value of $\sim$ 33 nm, which is the longest reported to date, to the best of our knowledge.

Methods

Time-resolved fluorescence (TRF) spectroscopy. TRF spectroscopy was carried out using *via* Pico Quant FluoTime 200 spectrometer. The NPLs were excited by a picosecond pulsed laser at the wavelength of 375 nm at low level intensity ($\approx$ 10 nJ/cm^2). Thus, the number of photogenerated excitons was set much smaller than one photon per NPL on the average ($< N > \ll 1$). The fluorescence decay curves were collected by TimeHarp time-correlated single-photon counting (TCSPC) unit. Then, we fitted the fluorescence decay curves to multiexponential decays through the FluoFit software by using the reconvolution mode of fitting to account for the instrument response function (IRF) of the excitation pulse.

Supporting Information

Synthesis and characterization of 4 monolayer CdSe/CdS core/crown nanoplateletes, the growth of MoS_2 flakes *via* chemical vapor deposition, sample characterization by atomic force microscopy. Time-resolved fluorescence decay curves from different positions of the samples along with their analyses. The numerical fitting of Förster resonance energy transfer efficiency.

Corresponding Author

* Email: volkan@stanfordalumni.org

Conflict of Interest

The authors declare no financial competing financial interest.

Acknowledgment

The authors gratefully acknowledge the financial support in part from Singapore National Research Foundation under the programs of NRF-NRFI2016-08 and the Science and Engineering Research Council, Agency for Science, Technology and Research (A*STAR) of Singapore and in part from TUBITAK 114F326 and 115E679. H.V.D. also acknowledges support from TUBA. K.G. and O.E. acknowledge support from TUBITAK BIDEB.

References

(1) Eda, G.; Maier, S. A. Two-Dimensional Crystals: Managing Light for Optoelectronics. *ACS Nano* **2013**, *7*, 5660–5665.

(2) Xia, F.; Wang, H.; Xiao, D.; Dubey, M.; Ramasubramaniam, A. Two-Dimensional Material Nanophotonics. *Nat. Photonics* **2014**, *8*, 899–907.

(3) Wang, Q. H.; Kalantar-Zadeh, K.; Kis, A.; Coleman, J. N.; Strano, M. S. Electronics and Optoelectronics of Two-Dimensional Transition Metal Dichalcogenides. *Nat. Nanotechnol.* **2012**, *7*, 699–712.

(4) Ponraj, J. S.; Xu, Z.-Q.; Dhanabalan, S. C.; Mu, H.; Wang, Y.; Yuan, J.; Li, P.; Thakur, S.;

Ashrafi, M.; Mccoubrey, K.; Zhang, Y.; Li, S.; Zhang, H.; Bao, Q. Photonics and Optoelectronics of Two-Dimensional Materials beyond Graphene. *Nanotechnology* **2016**, *27*, 462001.

(5) Bonaccorso, F.; Sun, Z.; Hasan, T.; Ferrari, A. C. Graphene Photonics and Optoelectronics. **2010**, *4*, 611–622.

(6) Lee, J.; Dak, P.; Lee, Y.; Park, H.; Choi, W.; Alam, M. A.; Kim, S. Two-Dimensional Layered MoS2 Biosensors Enable Highly Sensitive Detection of Biomolecules. *Sci. Rep.* **2015**, *4*, 7352.

(7) Chen, Y.; Tan, C.; Zhang, H.; Wang, L. Two-Dimensional Graphene Analogues for Biomedical Applications. *Chem. Soc. Rev.* **2015**, *44*, 2681–2701.

(8) Song, Y.; Luo, Y.; Zhu, C.; Li, H.; Du, D.; Lin, Y. Recent Advances in Electrochemical Biosensors Based on Graphene Two-Dimensional Nanomaterials. *Biosens. Bioelectron.* **2016**, *76*, 195–212.

(9) Ithurria, S.; Dubertret, B. Quasi 2D Colloidal CdSe Platelets with Thicknesses Controlled at the Atomic Level. *J. Am. Chem. Soc.* **2008**, *130*, 16504–16505.

(10) Ithurria, S.; Tessier, M. D.; Mahler, B.; Lobo, R. P. S. M.; Dubertret, B.; Efros, A. L. Colloidal Nanoplatelets with Two-Dimensional Electronic Structure. *Nat. Mater.* **2011**, *10*, 936–941.

(11) Olutas, M.; Guzelturk, B.; Kelestemur, Y.; Yeltik, A.; Delikanli, S.; Demir, H. V. Lateral Size-Dependent Spontaneous and Stimulated Emission Properties in Colloidal CdSe Nanoplatelets. *ACS Nano* **2015**, *9*, 5041–5050.

(12) Guzelturk, B.; Kelestemur, Y.; Olutas, M.; Delikanli, S.; Demir, H. V. Amplified Spontaneous Emission and Lasing in Colloidal Nanoplatelets. *ACS Nano* **2014**, *8*, 6599–6605.

(13) Kunneman, L. T.; Tessier, M. D.; Heuclin, H.; Dubertret, B.; Aulin, Y. V.; Grozema, F. C.; Schins, J. M.; Siebbeles, L. D. A. Bimolecular Auger Recombination of Electron-Hole Pairs in Two-Dimensional CdSe and CdSe/CdZnS Core/Shell Nanoplatelets. *J. Phys. Chem. Lett.* **2013**, *4*, 3574–3578.

(14) Tessier, M. D.; Javaux, C.; Maksimovic, I.; Loriette, V.; Dubertret, B. Spectroscopy of Single CdSe Nanoplatelets. *ACS Nano* **2012**, *6*, 6751–6758.

(15) Vitukhnovsky, A. G.; Lebedev, V. S.; Selyukov, A. S.; Vashchenko, A. A.; Vasiliev, R. B.;

Sokolikova, M. S. Electroluminescence from Colloidal Semiconductor CdSe Nanoplatelets in Hybrid Organic-Inorganic Light Emitting Diode. *Chem. Phys. Lett.* **2015**, *619*, 185–188.

(16) Prudnikau, A.; Chuvilin, A.; Artemyev, M. CdSe-CdS Nanoheteroplatelets with Efficient Photoexcitation of Central CdSe Region through Epitaxially Grown CdS Wings. *J. Am. Chem. Soc.* **2013**, *135*, 14476–14479.

(17) Kramer, I. J.; Levina, L.; Debnath, R.; Zhitomirsky, D.; Sargent, E. H. Solar Cells Using Quantum Funnels. *Nano Lett.* **2011**, *11*, 3701–3706.

(18) Guzelturk, B.; Demir, H. V. Near-Field Energy Transfer Using Nanoemitters For Optoelectronics. *Adv. Funct. Mater.* **2016**, *26*, 8158–8177.

(19) Forster, T. Energiewanderung Und Fluoreszenz. *Naturwissenschaften* **1946**, *33*, 166–175.

(20) Olutas, M.; Guzelturk, B.; Kelestemur, Y.; Gungor, K.; Demir, H. V. Highly Efficient Nonradiative Energy Transfer from Colloidal Semiconductor Quantum Dots to Wells for Sensitive Noncontact Temperature Probing. *Adv. Funct. Mater.* **2016**, *26*, 2891–2899.

(21) Rowland, C. E.; Fedin, I.; Zhang, H.; Gray, S. K.; Govorov, A. O.; Talapin, D. V.; Schaller, R. D. Picosecond Energy Transfer and Multiexciton Transfer Outpaces Auger Recombination in Binary CdSe Nanoplatelet Solids. *Nat. Mater.* **2015**, *14*, 484–489.

(22) Guzelturk, B.; Olutas, M.; Delikanli, S.; Kelestemur, Y.; Erdem, O.; Demir, H. V. Nonradiative Energy Transfer in Colloidal CdSe Nanoplatelet Films. *Nanoscale* **2015**, *7*, 2545–2551.

(23) Chen, Z.; Berciaud S.; Nuckolls C.; Heinz, T. F.; Brus, L. E. Energy Transfer from Individual Semiconductor Nanocrystals to Graphene. *ACS Nano* **2010**, *4*, 2964–2968.

(24) Gaudreau, L.; Tielrooij, K. J.; Prawiroatmodjo, G. E. D. K.; Osmond, J.; De Abajo, F. J. G.; Koppens, F. H. L. Universal Distance-Scaling of Nonradiative Energy Transfer to Graphene. *Nano Lett.* **2013**, *13*, 2030–2035.

(25) Lightcap, I. V.; Kamat, P. V. Fortification of CdSe Quantum Dots with Graphene Oxide. Excited State Interactions and Light Energy Conversion. *J. Am. Chem. Soc.* **2012**, *134*, 7109–7116.

(26) Yeltik, A.; Kucukayan-Dogu, G.; Guzelturk, B.; Fardindoost, S.; Kelestemur, Y.; Demir, H. V. Evidence for Nonradiative Energy Transfer in Graphene-Oxide-Based Hybrid Structures. *J. Phys. Chem. C* **2013**, *117*, 25298–25304.

(27) Shafran, E.; Mangum, B. D.; Gerton, J. M. Energy Transfer from an Individual Quantum

Dot to a Carbon Nanotube. *Nano Lett.* **2010**, *10*, 4049–4054.

(28) Prins, F.; Goodman, A. J.; Tisdale, W. A. Reduced Dielectric Screening and Enhanced Energy Transfer in Single- and Few-Layer MoS_2. *Nano Lett.* **2014**, *14*, 6087–6091.

(29) Raja, A.; Montoya-Castillo, A.; Zultak, J.; Zhang, X. X.; Ye, Z.; Roquelet, C.; Chenet, D. A.; Van Der Zande, A. M.; Huang, P.; Jockusch, S.; Hone, J.; Reichman, D. R.; Brus, L. E.; Heinz, T. F. Energy Transfer from Quantum Dots to Graphene and MoS_2: The Role of Absorption and Screening in Two-Dimensional Materials. *Nano Lett.* **2016**, *16*, 2328–2333.

(30) Goodfellow, K. M.; Chakraborty, C.; Sowers, K.; Waduge, P.; Wanunu, M.; Krauss, T.; Driscoll, K.; Vamivakas, A. N. Dimensional Semiconductor Distance-Dependent Energy Transfer between CdSe / CdS Quantum Dots and a Two-Dimensional Semiconductor. *Appl. Phys. Lett.* **2016**, *021101*, 1–5.

(31) Federspiel, F.; Froehlicher, G.; Nasilowski, M.; Pedetti, S.; Mahmood, A.; Doudin, B.; Park, S.; Lee, J. O.; Halley, D.; Dubertret, B.; Gilliot, P.; Berciaud, S. Distance Dependence of the Energy Transfer Rate from a Single Semiconductor Nanostructure to Graphene. *Nano Lett.* **2015**, *15*, 1252–1258.

(32) Abécassis, B.; Tessier, M. D.; Davidson, P.; Dubertret, B. Self-Assembly of CdSe Nanoplatelets into Giant Micrometer-Scale Needles Emitting Polarized Light. *Nano Lett.* **2014**, *14*, 710–715.

(33) Kelestemur, Y.; Dede, D.; Gungor, K.; Usanmaz, C. F.; Erdem, O.; Demir, H. V. Alloyed Heterostructures of $CdSe_xS_{1-x}$ Nanoplatelets with Highly Tunable Optical Gain Performance. *Chem. Mater.* **2017**, *29*, 4857–4865.

(34) Lee, C.; Yan, H.; Brus, L.; Heinz, T.; Hone, J.; Ryu, S. Anomalous Lattice Vibrations of Single-and Few-Layer MoS_2. *ACS Nano* **2010**, *4*, 2695–2700.

(35) Li, H.; Zhang, Q.; Yap, C. C. R.; Tay, B. K.; Edwin, T. H. T.; Olivier, A.; Baillargeat, D. From Bulk to Monolayer MoS_2: Evolution of Raman Scattering. *Adv. Funct. Mater.* **2012**, *22*, 1385–1390.

(36) Mak, K. F.; Lee, C.; Hone, J.; Shan, J.; Heinz, T. F. Atomically Thin MoS_2: A New Direct-Gap Semiconductor. *Phys. Rev. Lett.* **2010**, *136805*, 2–5.

(37) Peng, X.; Misewich, J. A.; Wong, S. S.; Sfeir, M. Y. Efficient Charge Separation in Multidimensional Nanohybrids. *Nano Lett.* **2011**, *11*, 4562–4568.

(38) Chanyawadee, S.; Lagoudakis, P. G.; Harley, R. T.; Charlton, M. D. B.; Talapin, D. V.;

Huang, H. W.; Lin, C. H. Increased Color-Conversion Efficiency in Hybrid Light-Emitting Diodes Utilizing Non-Radiative Energy Transfer. *Adv. Mater.* **2010**, *22*, 602–606.

(39) Rindermann, J. J.; Pozina, G.; Monemar, B.; Hultman, L.; Amano, H.; Lagoudakis, P. G. Dependence of Resonance Energy Transfer on Exciton Dimensionality. *Phys. Rev. Lett.* **2011**, *107*, 1–5.

(40) Lin, T. N.; Huang, L. T.; Shu, G. W.; Yuan, C. T.; Shen, J. L.; Lin, C. a J.; Chang, W. H.; Chiu, C. H.; Lin, D. W.; Lin, C. C.; Kuo, H. C. Distance Dependence of Energy Transfer from InGaN Quantum Wells to Graphene Oxide. *Opt. Lett.* **2013**, *38*, 2897–2899.

(41) Agranovich, V. M.; Rupasov, V. I.; Silvestri, L. Hybrid Resonant Organic-Inorganic Nanostructures for Novel Light Emitting Devices and Solar Cells. *Phys. Status Solidi Curr. Top. Solid State Phys.* **2010**, *7*, 1684–1687.

(42) Becker, K.; Lupton, J. M.; Müller, J.; Rogach, A. L.; Talapin, D. V.; Weller, H.; Feldmann, J. Electrical Control of Förster Energy Transfer. *Nat. Mater.* **2006**, *5*, 777–781.

(43) Kuhn, H. Classical Aspects of Energy Transfer in Molecular Systems. *J. Chem. Phys.* **1970**, *53*, 101–108.

(44) Yu, Y.-J.; Kim, K. S.; Nam, J.; Kwon, S. R.; Byun, H.; Lee, K.; Ryou, J.-H.; Dupuis, R. D.; Kim, J.; Ahn, G.; Ryu, S.; Ryu, M.-Y.; Kim, J. S. Temperature-Dependent Resonance Energy Transfer from Semiconductor Quantum Wells to Graphene. *Nano Lett.* **2015**, *15*, 896–902.

(45) Govorov, A. O.; Carmeli, I. Hybrid Structures Composed of Photosynthetic System and Metal Nanoparticles: Plasmon Enhancement Effect. *Nano Lett.* **2007**, *7*, 620–625.

(46) Hernández-Martínez, P. L.; Govorov, A. O. Exciton Energy Transfer between Nanoparticles and Nanowires. *Phys. Rev. B - Condens. Matter Mater. Phys.* **2008**, *78*, 1–7.

(47) Scott, R.; Heckmann, J.; Prudnikau, A. V.; Antanovich, A.; Mikhailov, A.; Owschimikow, N.; Artemyev, M.; Climente, J. I.; Woggon, U.; Grosse, N. B.; Achtstein, A. W. Directed Emission of CdSe Nanoplatelets Originating from Strongly Anisotropic 2D Electronic Structure. *Nat. Nanotechnol.* **2017**, *12*, 1155–1160.

(48) Gao, Y.; Weidman, M. C.; Tisdale, W. A. CdSe Nanoplatelet Films with Controlled Orientation of Their Transition Dipole Moment. *Nano Lett.* **2017**, *17*, 3837–3843.

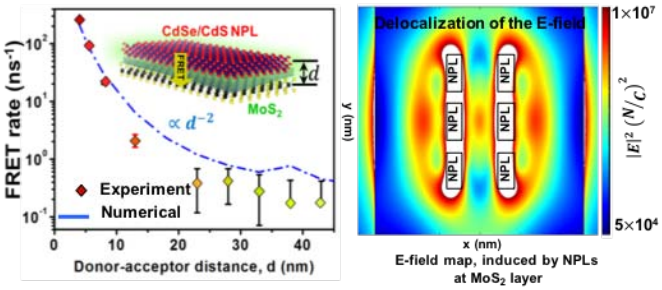
CdSe/CdS NPL
FRET
d
MoS2
∝ d−2
Experiment
Numerical
FRET rate (ns−1)
Donor-acceptor distance, d (nm)
Delocalization of the E-field
NPL
y (nm)
x (nm)
1×10^7
5×10^4
|E|^2 (N/C)^2
E-field map, induced by NPLs
at MoS2 layer